Cellulose (2019) 26:3339–3358
https://doi.org/10.1007/s10570-019-02314-2

ORIGINAL RESEARCH

Eco-friendly cellulose–bentonite porous composite hydrogels for adsorptive removal of azo dye and soilless culture

Shella Permatasari Santoso · Alfin Kurniawan · Felycia Edi Soetaredjo · Kuan-Chen Cheng · Jindrayani Nyoo Putro · Suryadi Ismadji · Yi-Hsu Ju

Received: 11 October 2018 / Accepted: 1 February 2019 / Published online: 9 February 2019

Abstract Cellulose hydrogels are a three-dimensional (3D) network of cross-linked cellulosic fibers that have the potential to be used as an environmentally friendly adsorbent. Bentonite clay is also a low cost inorganic adsorbent and has been frequently used to remove toxic organic compounds from water. However, in most cases, bentonite is often ground to a fine powder to increase the available surface area for adsorption, which makes its separation from an aqueous mixture difficult. In this study, we demonstrate straightforward fabrication of cellulose–bentonite (CB) porous composite hydrogels and its potential as an adsorbent for dye removal. The preparation, formation mechanism, and the adsorption performance of CB hydrogels with homogeneously dispersed clay particles were investigated. The adsorption isotherms, kinetics, and thermodynamics of CB hydrogels were examined toward an anionic dye pollutant (Congo red). The results showed that physisorption is the predominant adsorption mechanism of Congo red onto CB hydrogels. The equilibrium adsorption and kinetic data were well fitted by Langmuir isotherm and pseudo-second-order models, respectively. The theoretical maximum adsorption capacity of the CB30 hydrogel with 30 wt% clay loading was found to be 45.77 mg g^{-1}, which was the highest value among other fabricated hydrogels. We also demonstrate the potential application of these CB hydrogels as soilless growing media for legume (*Vigna radiata* L.) and small flowering plants (*Arabidopsis thaliana*).

Electronic supplementary material The online version of this article (https://doi.org/10.1007/s10570-019-02314-2) contains supplementary material, which is available to authorized users.

Shella Permatasari Santoso and Alfin Kurniawan have contributed equally to this work.

S. P. Santoso (✉) · F. E. Soetaredjo · S. Ismadji
Department of Chemical Engineering, Widya Mandala Surabaya Catholic University, Kalijudan 37, Surabaya 60114, Indonesia
e-mail: shella_p5@yahoo.com

A. Kurniawan · J. N. Putro · Y.-H. Ju
Department of Chemical Engineering, National Taiwan University of Science and Technology, No. 43, Sec. 4, Keelung Rd., Taipei 10607, Taiwan

K.-C. Cheng
Institute of Biotechnology, National Taiwan University, No. 1, Sec. 4, Roosevelt Rd., Taipei 10617, Taiwan

K.-C. Cheng
Graduate Institute of Food Science and Technology, National Taiwan University, No. 1, Sec. 4, Roosevelt Rd., Taipei 10617, Taiwan

K.-C. Cheng
Department of Medical Research, China Medical University Hospital, China Medical University, No. 91, Hsueh-Shih Rd., Taichung 40402, Taiwan

Graphical abstract

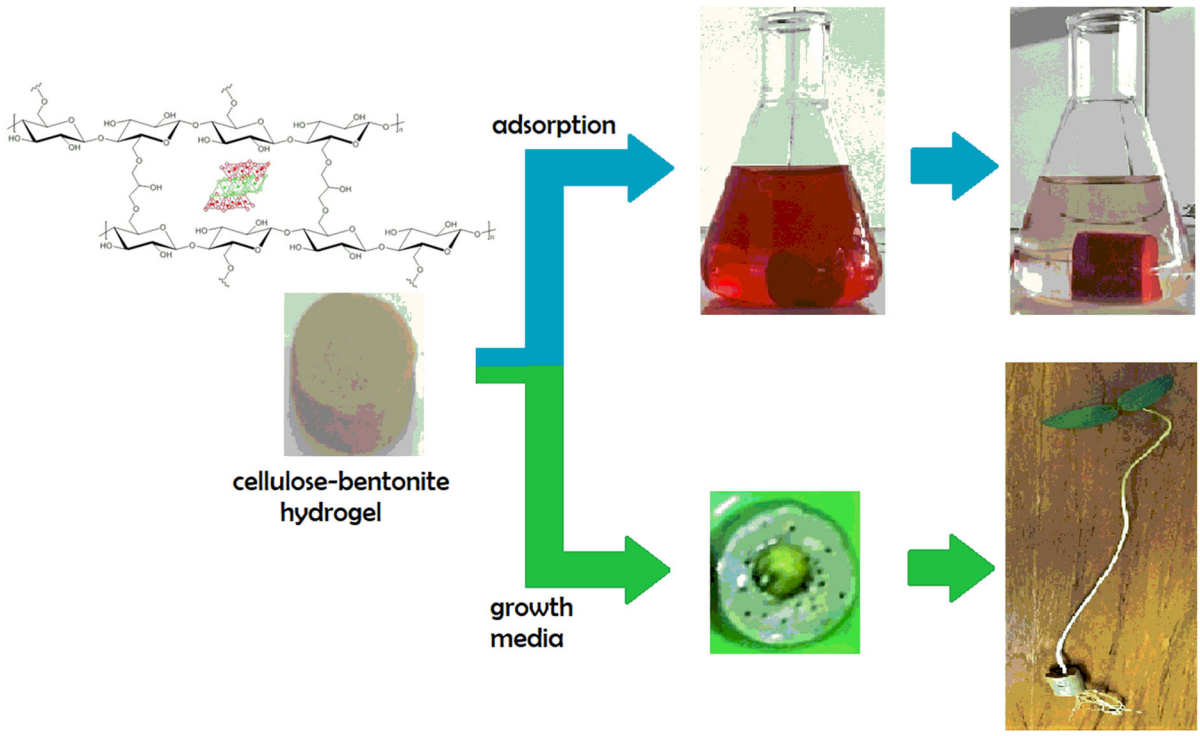

Keywords Cellulose composite · Hydrogel · Bentonite · Adsorption · Soilless culture

Introduction

Hydrogels represent a physically or chemically cross-linked 3D networks based on hydrophilic macromonomers that have found important applications in many fields. Their exceptional ability to accommodate large amounts of water and swell without loss of structural integrity makes hydrogel a particularly attractive material for growing plants in both ornamental and agricultural scales (Takács et al. 2010; Chang and Zhang 2011; Montesano et al. 2015; Mohammadi-Khoo et al. 2016). Hydrogels have also attracted considerable attention as an effective adsorbent for water and wastewater treatment, biomaterials such as wound dressings and drug delivery vehicles, biosensors, and many other applications (Li et al. 2015; Shen et al. 2016; Tu et al. 2017). Cellulose is one of the most widely used biopolymers for preparing hydrogels and other sustainable products because of its natural abundance, low cost, renewability, and environmental friendliness (Demitri et al. 2014; Shen et al. 2016). Cellulose is a linear polymer composed of repeating β-(1 → 4)-linked D-glucose units where its transformation into hydrogel involves partial or complete dissolution of cellulosic fibers. Despite its simple linear structure, cellulose does not readily dissolve in many commonly used solvents including water. A convenient strategy for cellulose dissolution is by using a pre-cooled alkali/urea aqueous system. Such environmentally benign, non-derivatizing solvent system can swell and dissolve cellulose rapidly by interrupting its supramolecular structure. Therefore, cellulose dissolved in this fashion can be cross-linked into a 3D network to form hydrogel (Chang and Zhang 2011; Olsson and Westman 2013; Zhang et al. 2013; Maitra and Shukla 2014).

In this work, cellulose hydrogel was used to remove a refractory dye Congo red (CR) from water. CR is a water-soluble conjugated diazo dye containing amine ($–NH_2$) and sulfonic acid ($–SO_3$) groups that are

widely used by biologists to stain cell walls and visualize microorganisms. This synthetic dye has also found commercial success as a textile colorant, but its practice was abandoned because it can degrade rapidly in the presence of light. Also, care must be taken when disposing CR because of its carcinogenic and mutagenic effects, which can adversely affect aquatic life and humans (Bhattacharya et al. 2011; Patel and Vashi 2012; Li et al. 2015).

The adsorption capability of cellulose-based hydrogels can be improved by incorporation of clay materials, such as bentonite. Bentonite, an aluminum phyllosilicate rock composed mainly of montmorillonite clay mineral, is well known as an effective adsorbent in water and wastewater treatment (Sing 1998; Volzone and Garrido 2001; Adzmi et al. 2012; Suwandi et al. 2012). However, the powdered shape of such adsorbent cannot easily be recovered from the liquid phase because filtration or centrifugation techniques are often impractical, and thus restricts its potential applications to many industrial situations. Research efforts have therefore been directed toward incorporating clay materials into various 2D and 3D structures to facilitate easy separation and achieve higher adsorption capacity. For instance, Daraei et al. (2013) synthesized a PVDF thin film composite microfiltration membrane coated with organoclay/chitosan nanocomposite for methylene blue (MB) dye removal from water where efficient adsorption performance of organoclay particles provides superior dye removal rather than bare chitosan. The incorporation of Cloisite 30B nanoclay into PVA/chitosan/agar–agar tripolymeric nanohydrogels has been shown to shorten the equilibrium contact time and significantly enhance the removal efficiency of the hydrogel toward MB and Rhodamine B dyes (Sarkar et al. 2018). Bhattacharyya and Ray (2015) demonstrated that the inclusion of 1 wt% nanosized bentonite filler into composite hydrogel of poly(acrylic acid) and poly(ethylene glycol) enhances the equilibrium swelling ratio and consequently the adsorption capacity of the hydrogel toward CR and methyl violet dyes. A hydrogel based on cross-linked networks of cellulose, carboxymethyl cellulose, and epoxidized clay with superabsorbent and superior mechanical properties has been prepared by Peng et al. (2016) for highly efficient adsorption of MB. Herein, we present a simple and robust approach to incorporate unmodified bentonite clay into cellulose hydrogel to improve its adsorption capacity for a practical and scalable adsorption process. The use of unmodified natural clay instead of organoclay has the advantage that the mass production of adsorbent material and scale-up of the sorption process would become simpler and more economically feasible.

In the present work, cellulose-based hydrogel and bentonite clay were employed for the preparation of a composite adsorbent because they are cheap, environmental friendly, abundantly available, and easy to prepare and/or modify compared with nanostructured adsorbents, such as graphene oxide, metal organic frameworks, and metal oxides (e.g., TiO_2, ZrO_2, ZnO_2, Fe_2O_3, Al_2O_3, and SnO_2) (Sun et al. 2014; Pham et al. 2015; Bahranowski et al. 2017). Hydrogel was chosen as the adsorbent material because of its ability to absorb large amounts of water rapidly and maintain water-saturated state for a long duration (Ahmed 2015), in addition to its easy separation from aqueous solution for reuse compared to the above-mentioned nanostructured adsorbents. Moreover, the versatility and ease of surface functionalization with reactive groups (e.g., hydroxyl, carboxyl, amino, etc.) as well as swelling of the 3D cross-linked network structure of the hydrogel enable unique selectivity and remarkable adsorption capacity toward organic and inorganic compounds (Chen et al. 2016). The aim of this work was to fabricate cellulose–bentonite (CB) porous composite hydrogels and to investigate the composite formation mechanism. The structure and properties of the prepared composite hydrogels were characterized by scanning electron microscopy (SEM), Fourier transform infrared spectroscopy (FTIR), thermogravimetric analysis (TGA), and X-ray diffraction (XRD). The adsorption characteristics of the prepared cellulose hydrogels with and without bentonite clay toward CR dye at different temperatures and adsorbent doses were investigated. To the best of our knowledge, there has been no report demonstrating the fabrication of CB hydrogels and their application to adsorptive removal of CR from aqueous solution. The adsorption equilibrium isotherms, kinetics, and thermodynamics were also studied to elucidate the nature and mechanism of CR dye adsorption onto CB hydrogels. In addition, we also tested the capability of these porous composite hydrogels as a solid soilless substrate to promote seedling germination in the model plant mung bean

(*Vigna radiata* L.) and mouse-ear cress (*Arabidopsis thaliana*).

Materials and methods

Materials

CR (CI 22,120; dye content: 97%; chemical formula: $C_{32}H_{22}N_6Na_2O_6S_2$; M.W.: 696.67 g mol^{-1}) was purchased as analytical grade from Sigma-Aldrich. Sodium hydroxide (NaOH, 96% purity) was purchased from Yakuri Pure Chemical (Kyoto, Japan). Sodium chloride (NaCl, 99.5% purity) was purchased from Showa Chemical (Tokyo, Japan). Urea (NH_2-$CONH_2$, 98% purity) and epichlorohydrin (ECH, 98% purity) were purchased from Sigma-Aldrich (Steinheim, Germany). All chemicals were used as received without further treatment.

Preparation of cellulose hydrogel (CB0)

Cellulose hydrogel was prepared from laboratory filter paper (Whatman #1). The filter paper was soaked overnight in tap water and then shredded into pulp with a blender. Subsequently, the pulp was filtered and dried in an oven overnight. Dried pulp was further grounded using a blender to obtain smaller filter paper fibers. An aqueous solution of NaOH/urea was freshly prepared by mixing 7 wt% NaOH and 12 wt% urea, which was pre-cooled to − 10 °C. Shredded dried pulp (3 wt%) was then added into a 100 mL of NaOH/urea solution and mixed well under vigorous stirring. The stirring was continued for 30 min at ambient temperature to obtain a transparent viscous solution. Afterward, the cellulose solution was cross-linked by adding 5% (w/v) ECH, stirred for 20 min at ambient temperature, centrifuged, and poured into a cylindrical mold (diameter = 15 mm; height = 0.3 mm). The molds were then placed in a water bath maintained at 60 °C for 30 min to initiate the cross-linking reaction. The resulting hydrogels were gently removed from the mold and washed repeatedly with water to remove excess chemicals. After washing, the hydrogels were lyophilized and kept in the desiccators until further use.

Preparation of homoionic bentonite clay

Bentonite deposits were obtained from a mining area near Pacitan region of southwestern East Java Province and then dried in an oven at 110 °C overnight. The dried bentonite was crushed into a fine powder with a hammer mill and sieved using a 100-mesh screen, followed by soaking in a 3% (v/v) hydrogen peroxide solution for 24 h to remove organic impurities. The purified bentonite was then rinsed several times with distilled water and dried in an oven at 110 °C overnight. Subsequently, 10 wt% of dried bentonite powder was homoionized by stirring in a 100 mL of 3 M NaCl solution for 48 h. Afterward, the mixture was allowed to settle where the suspended clay particles were collected and washed several times with deionized water to remove excess chloride ions. The modified bentonite was oven-dried at 110 °C for 24 h and stored in a desiccator for further use.

Preparation of CB hydrogels

The CB hydrogels were prepared by adding a known amount of homoionic clay powder (i.e., 10, 20, and 30 wt%) into previously prepared cellulose solution. The CB mixture was then stirred for 30 min at ambient temperature prior to the addition of ECH. The mixture was then poured into cylindrical molds and heated at 60 °C in a water bath to form hydrogel. The resulted composite hydrogels were coded as CB10, CB20, and CB30 according to the clay content.

Water retention capacity

The water retention capacity (WRC) or swelling degree of the prepared hydrogels was determined by the gravimetric method according to the following procedure: a known weight of dried hydrogel samples was immersed in beakers containing 200 mL of DI water at room temperature for 48 h. The excess of water at the surface of the swollen hydrogel was gently blotted using a filter paper, then its weight was measured with an analytical balance and recorded as W_s. The swollen hydrogel was then dried in an oven at 105 °C until the weight was constant to obtain W_d. All swelling experiments were repeated three times and the results are expressed as mean ± standard deviation (SD). The WRC of the hydrogels was calculated using Eq 1:

$$\text{WRC (g/g)} = \frac{W_s - W_d}{W_d} \quad (1)$$

Characterization of the hydrogels

Nitrogen sorption

Nitrogen adsorption/desorption isotherms were measured at 77 K on a Quadrasorb SI analyzer (Quantachrome Instruments) to determine the Brunauer–Emmett–Teller specific surface area (S_{BET}) of the samples. Before the measurements, the samples were subjected to degassing at 423 K in vacuum for at least 6 h. Measurements were conducted over a relative pressure (P/P_0) range of 0.005–0.995. The S_{BET} values were determined from experimental points on the adsorption branch of the isotherm in the P/P_0 range 0.05–0.30. The total pore volume, V_t, was obtained from the amount of adsorbed N_2 at a P/P_0 value of 0.995.

SEM

SEM images of the prepared hydrogels were obtained with a JEOL (JSM-6500F, Tokyo, Japan) field emission SEM at an accelerating voltage of 10 kV. Before SEM imaging, the freeze-dried hydrogel samples were immersed in liquid nitrogen for a few minutes and fractured into small pieces. The fractured hydrogel pieces were then fixed onto a metallic holder using double-sided adhesive carbon tape and sputter-coated with a very thin layer of platinum-palladium alloy using a JEOL auto fine coater (JEC-3000FC). The surface chemical composition analysis by energy dispersive X-ray (EDX) spectroscopy was carried out using an Oxford Instruments EDX attachment on the SEM instrument and operated by INCA software.

XRD

Crystalline structure of the prepared hydrogels was analyzed by XRD using a Bruker D2 Phaser desktop X-ray diffractometer at room temperature. The diffraction patterns were collected in the 2θ range from 10° to 50° with a step size of 0.05° and a step time of 0.5 s using Cu Kα radiation (λ = 1.5418 Å) at 30 kV and 10 mA. The cellulose crystallinity index (CrI) of the prepared hydrogel samples was determined from the ratio of the maximum intensity of the (200) peak (I_{200}) at approximately 2θ = 22.5° to the minimum intensity of amorphous phase (I_{AM}) taken at 2θ angle between the (200) and ($1\bar{1}0$) peaks according to the Segal method (Segal et al. 1959).

TGA

The thermal stability of the prepared hydrogels was analyzed by TGA using a Perkin-Elmer Diamond TG/DTA thermal analyzer under N_2 gas flow (50 mL/min) and a heating rate of 10 °C min^{-1} from room temperature to 600 °C.

Attenuated total reflectance (ATR)-FTIR

The surface functional groups of the hydrogels were analyzed using ATR-FTIR spectroscopy. All spectra were collected in transmission mode on a Bio-Rad Model FTS-3500 GX spectrometer equipped with a diamond ATR accessory with an accumulation of 128 scans and a resolution of 4 cm^{-1} in the wavenumber range from 4000 to 400 cm^{-1}.

Batch adsorption experiments

Adsorption experiments were conducted in batch mode, where CR dye was chosen as a model adsorbate to evaluate the adsorption performance of CB hydrogels. The dye stock solution (1000 mg L^{-1}) was freshly prepared by dissolving 1 g of dye powder into 1 L of distilled water. The dye stock solution was kept in a dark bottle to prevent light-induced degradation. The calibration curves were prepared by measuring the absorbance of dye solutions of known concentrations at a λ_{max} of 497 nm using a UV–Vis spectrophotometer (UV-1700 PharmaSpec, Shimadzu, Japan). For the adsorption equilibrium studies, a series of 100 mL of dye solution (50 mg L^{-1}) was prepared from the stock solution. Then, different amounts of small hydrogel pieces were introduced into a series of working dye solutions. The adsorption experiments were performed in a thermostated shaking water bath at three different temperatures (i.e., 30, 40, and 50 °C) for 24 h to reach equilibrium. The amount of dye adsorbed per unit mass of adsorbent, q_e (mg g^{-1}), was calculated by using Eq 2:

$$q_e = \frac{C_0 - C_e}{m} \times V \quad (2)$$

where C_0 is the initial dye concentration (mg L^{-1}), C_e is the equilibrium dye concentration (mg L^{-1}), m is the mass of adsorbent (g), and V is the volume of dye solution (L). All adsorption tests were carried out at pH = 7.

The kinetics of dye adsorption process at room temperature (30 °C) was studied by adding a known weight of prepared bulk hydrogels into a series of Erlenmeyer flasks containing 100 mL of dye solution at a concentration of 50 mg L^{-1}. At predetermined time intervals, aliquots (1 mL) of the samples were taken and the residual dye concentration in the liquid phase was subsequently measured using a UV–Vis spectrophotometer. The amount of dye adsorbed at time t (q_t, mg g^{-1}) was calculated using Eq 3.

$$q_t = \frac{C_0 - C_t}{m} \times V \quad (3)$$

Results and discussion

Formation mechanism of CB0 hydrogel and its composites with bentonite clay

In this study, cellulose hydrogel was fabricated by using ECH as a chemical cross-linker where the formation mechanism is proposed as follows: In the first step shown in Fig. 1, a transparent viscous cellulose solution was obtained by dissolving Whatman cellulose filter paper in a NaOH/urea aqueous solution pre-cooled to − 10 °C. In this solvent system, NaOH serves as a strong base to cleave the intra- and intermolecular hydrogen bonding of cellulose, resulting in cellulose swelling to a certain extent due to the penetration of alkali hydrates and free water molecules. Moreover, NaOH can also induce deprotonation of the OH group in cellulose chains, leading to the formation of a water-dissoluble inclusion complex and good dissolution of cellulose (Blasko et al. 1997). The existence of hydrotrope (i.e., urea) in the aqueous system prevents the aggregation of cellulose chains as the temperature rises to room temperature. In addition, urea can improve the solubility of disrupted cellulose chains through interacting with the hydrophobic part of cellulose and forming hydrogen bond with water, thus enabling cellulose to rapidly dissolve at ambient temperature (Olsson and Westman 2013; Zhang et al. 2013).

In the second step, the cross-linking reaction of free cellulose chains is carried out by adding ECH as a chemical cross-linker. In this regard, ECH is attacked by a nucleophile, which is an oxyanion generated from deprotonation of the OH group in the glycosyl residues of cellulose by an S_N2-type mechanism involving a two-step nucleophilic attack. The cross-linking reaction between cellulose chains and ECH molecules begins with the formation of 2,3-epoxypropyl ethers by reaction of the latter species with OH groups (Holmberg et al. 1994), followed by the opening of the epoxide ring via nucleophilic attack of oxyanions. This nucleophilic attack by oxyanion takes place at the C1 position of ECH. However, the polar bond between carbon and chlorine atoms results in epoxide ring closure (Pan and Ragauskas 2012; Olsson and Westman 2013). The second nucleophilic attack causes detachment of the Cl atom and reconstruction of the epoxy ring. The presence of H^+ ions from deprotonation of the OH group causes protonation of the ring-opened ECH and prevents its closure. In this reaction step, NaOH acts as not only a catalyst for the nucleophilic ring-opening of the epoxide group but also a dehydrochlorinating agent for conversion of the chlorohydrins to epoxide group (Medjitov et al. 1998).

In the third step, the ring-opened ECH molecules cross-linked cellulose chains to form a 3D network. In this reaction, the ring-opened ECH species leaves two electrophilic carbon atoms, which become the target for a nucleophilic attack by oxyanions generated from deprotonation of the OH group. When the cellulose structure becomes a connected network, the heating process was performed to transform into a hydrogel.

In the formation of the composite hydrogels CB10, CB20, and CB30, bentonite clay was added into the transparent cellulose solution at certain mass ratios before the addition of ECH. The bentonite particles were trapped between the cross-linked network structures of cellulose where free cellulose chains could not enter the silicate gallery of clay, as illustrated in Fig. 2. In this case, the viscosity of the cellulose solution caused the bentonite particles to be uniformly distributed in the solution. When the cellulose solution was solidified, the bentonite particles were trapped in the cross-linked cellulose networks to form composite hydrogels.

Step 1: Deprotonation and dissolution of cellulose fibers in NaOH/urea aqueous solution

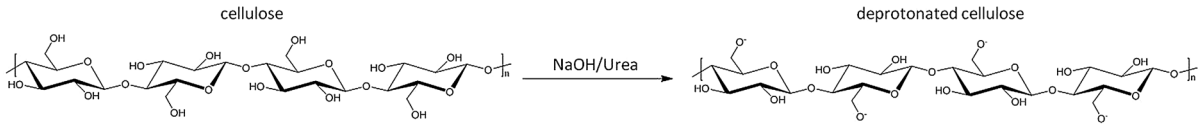

Step 2: The epoxide ring-opening reaction of ECH via a two-step nucleophilic attack involving an oxyanion moiety present in the glycosyl residues of cellulose by an S_N2-type mechanism

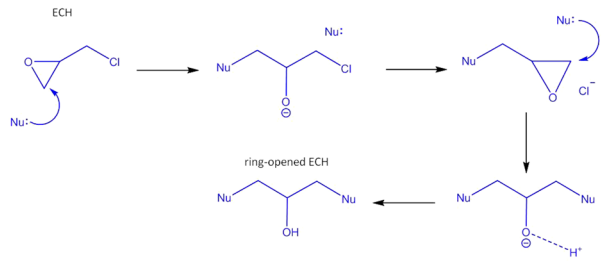

Step 3: The network structure of ECH cross-linked cellulose gel where the oxyanion groups in the glycosyl residues of cellulose interact with the electrophilic carbon atoms of the ring-opened ECH molecules

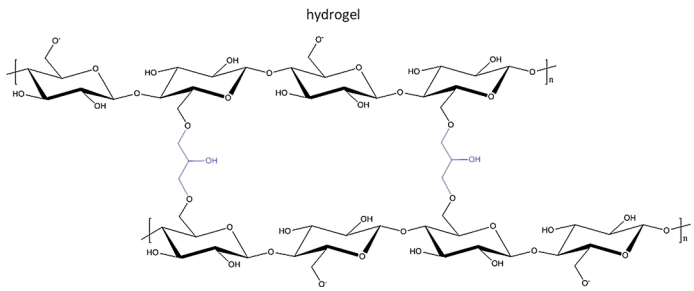

Fig. 1 The stepwise mechanism for the formation of CB0 hydrogel through cross-linking reaction of free cellulose chains with ECH under basic conditions

Textural properties and water retention capacities of CB hydrogels

The textural properties of pristine filter paper and CB hydrogels are presented in Table 1. The volume of gas adsorbed as a monolayer (V_m) indicates that CB0 hydrogel exhibited a marginally lower monolayer adsorption capacity than the pristine filter paper, which could be attributed to the shrinking of the porous structure as a result of cross-linked cellulose structure. The V_m values of the CB hydrogels (i.e., CB10, CB20, and CB30) increased by more than an order of magnitude compared to pristine filter paper and CB0 hydrogel. This implies that the enhanced gas adsorption on the composite hydrogels was attributed to the presence of bentonite particles embedded in the hydrogel matrix. The composite hydrogels CB10, CB20, and CB30 all showed higher S_{BET} values (29–51 $m^2\ g^{-1}$) compared to pristine filter paper (2.49 $m^2\ g^{-1}$) and CB0 hydrogel (2.41 $m^2\ g^{-1}$), suggesting that the addition of bentonite particles plays an important role in increasing the specific surface area and consequently the adsorption capacity of the composite hydrogels. The total pore volume (V_T) of all hydrogel samples is much lower than unity, indicating a Type I monolayer adsorption isotherm

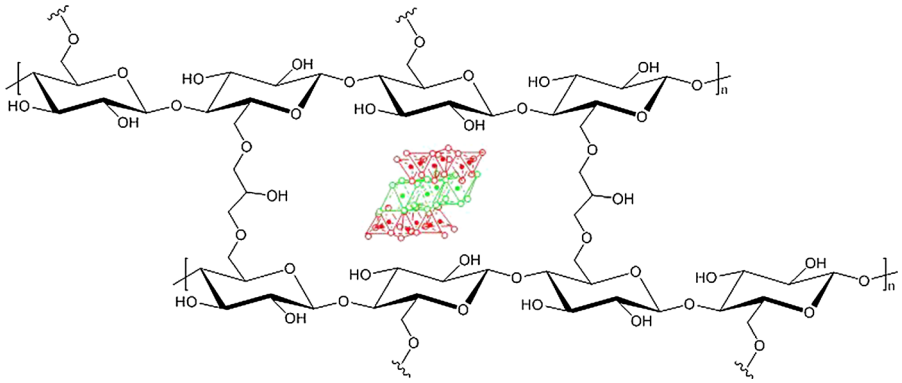

Fig. 2 Proposed structure of the CB hydrogel network containing bentonite clay. The solid blue line indicates opened ECH molecules cross-link free cellulose chains according to the stepwise mechanism described in Fig. 1. The schematic of the bentonite was represented by a 2:1 layer clay composed of repeating tetrahedral–octahedral–tetrahedral (T–O–T) layers as indicated by red and green colors (color figure online)

Table 1 Textural properties of pristine filter paper and CB hydrogels

Parameter[a]	Unit	Pristine filter paper	CB0	CB10	CB20	CB30
V_m	($cm^3\ g^{-1}$)	0.57	0.55	6.67	10.43	11.83
S_{BET}	($m^2\ g^{-1}$)	2.49	2.41	29.03	45.37	51.48
V_T	($\times\ 10^{-3}\ cm^3\ g^{-1}$)	1.2	1.2	14.8	23.2	26.4

[a]V_m and V_T were obtained from linear regression of the BET equation and the amount of N_2 adsorbed at $P/P_0 = 0.995$, respectively

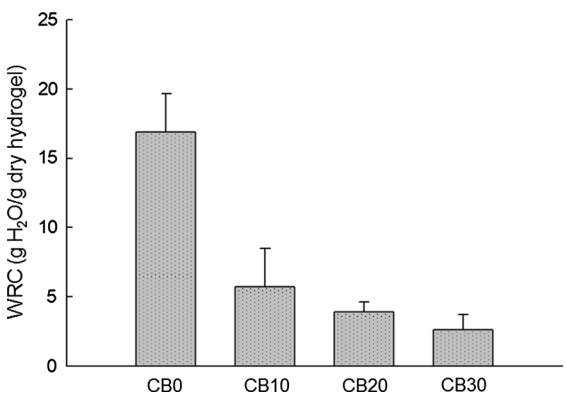

Fig. 3 The WRC of the CB hydrogels where error bars on the bar graphs represent the standard deviation from the mean

which can be well represented by Langmuir adsorption model (Brunauer et al. 1938; Sing 1998).

Figure 3 shows the WRC of the prepared hydrogel samples. The results indicated that the incorporation of bentonite particles decreased WRC of the hydrogel. Pure cellulose hydrogel, CB0, can retain a considerable amount of water, up to 16.86 ± 2.79 g H_2O per g of dry hydrogel. Meanwhile, the values of WRC were 5.74 ± 2.74, 3.89 ± 0.72, and 2.63 ± 1.07 g H_2O per g of dry hydrogel for CB10, CB20, and CB30 samples, respectively. In this case, the bentonite particles are embedded in and appear to fill cavities in the cellulose matrix, resulting in an increased cross-linking density of the composite hydrogels (Kaşgöz and Durmus 2008). Accordingly, the amount of water that can be retained inside the hydrogel becomes smaller with increasing clay content.

Characteristics of the prepared CB hydrogels

In the present work, pure cellulose as well as CB hydrogels were prepared from Whatman filter paper as the cellulose source. The characteristics of the resulted hydrogels (i.e., CB0, CB10, CB20, and CB30) were thoroughly examined by SEM–EDX, XRD, TGA, and FTIR analyses, and compared with that of pristine cellulose filter paper to study the properties modification.

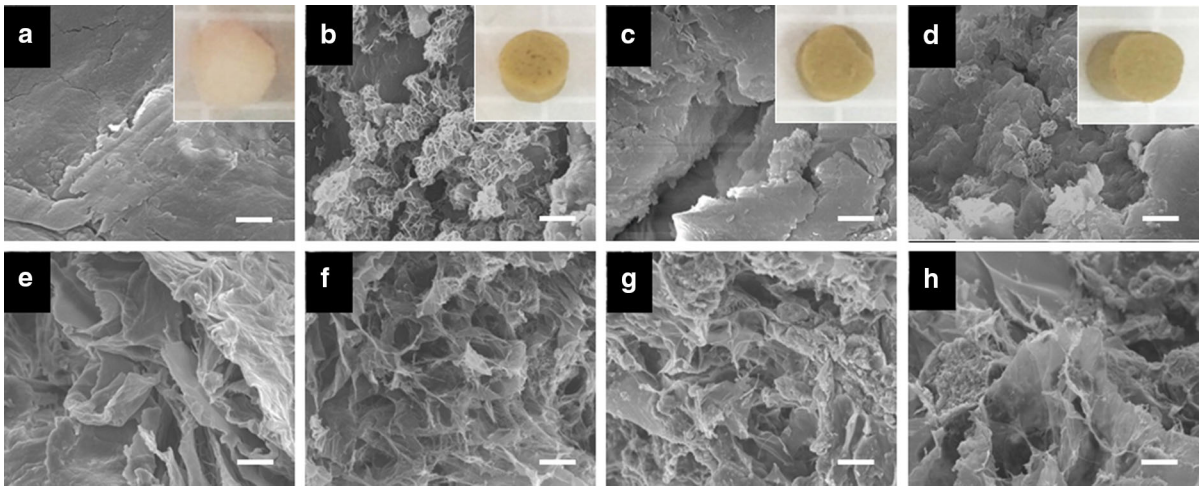

Fig. 4 SEM images of surfaces of CB hydrogels **a** CB0, **b** CB10, **c** CB20, and **d** CB30. Cross-sectional SEM images (**e**–**h**) of the fractured hydrogels corresponding to panels **a**–**d**. The insets in panels **a**–**d** show digital photographs of the hydrogels in the dry state. Scale bars are **a**–**d** 1 μm and **e**–**h** 10 μm

SEM–EDX analysis

The surface structures and cross sections of the cellulose hydrogels with and without bentonite were examined using SEM and the results are depicted in Fig. 4. The surface morphology of the pristine filter paper was also characterized, as shown in Supplemental Figure S1a. From this figure, the fibrous structure of cellulose in filter paper was observed before transforming into a hydrogel. After the formation of the hydrogel, the cellulose fiber surface becomes smoother without any apparent fibrous structure (Fig. 4a). The disappearance of the fibrous structure indicates swelling and dissolution of cellulose fibers due to disruption of the hydrogen bond network by NaOH/urea solution. Furthermore, the swollen cellulose fibers are connected to each other through the ECH cross-linker to form a 3D hydrogel network.

The surface morphologies of the composite hydrogels CB10, CB20, and CB30 are shown in Fig. 4b–d, respectively. As can be seen, the morphology of the three composite hydrogels shows no significant difference, which implies that the amount of clay loading does not cause a considerably change in the morphological structure of the hydrogels. Compared with the CB0 hydrogel (Fig. 4a), CB10, CB20, and CB30 hydrogels have rough surfaces because of the presence of bentonite particles embedded in the cellulose network. Higher magnification top-view SEM images of these hydrogels are displayed in Supplemental Figure S1b–d. It can be seen that all the composite hydrogels exhibit a dense structure, which could be ascribed to the swollen cellulose fibers acted as a filler in the hydrogel matrix. Also, very small pores with a few to tens of nanometers in size can be observed on the surface of the hydrogels (denoted by the black spots in the SEM images), which contribute to larger S_{BET} values compared to that of CB0 hydrogel. In this regard, the surface porosity of the composite hydrogels was developed due to the presence of bentonite particles. The cross-sectional SEM images were also taken to get a closer look into the porous interior structure of the hydrogels, as depicted in Fig. 4e–h. It can be clearly observed that all the hydrogels exhibited a sponge-like macroporous structure with irregularly shaped pores that are a few microns in size. It was also noticed that the porous interior structure of the hydrogel was well preserved even at 30% of clay loading, which suggested the homogeneous distribution of the clay with no agglomeration in the cross-linked cellulose networks. Furthermore, the incorporation of bentonite particles causes the color of the hydrogel gradually turned from opaque white to pale brown and then to yellow-brownish with an increase in clay loading from 10 to 30%, as displayed in the inset photographs of Fig. 4a–d.

The presence of bentonite particles uniformly distributed in the hydrogel matrix was further

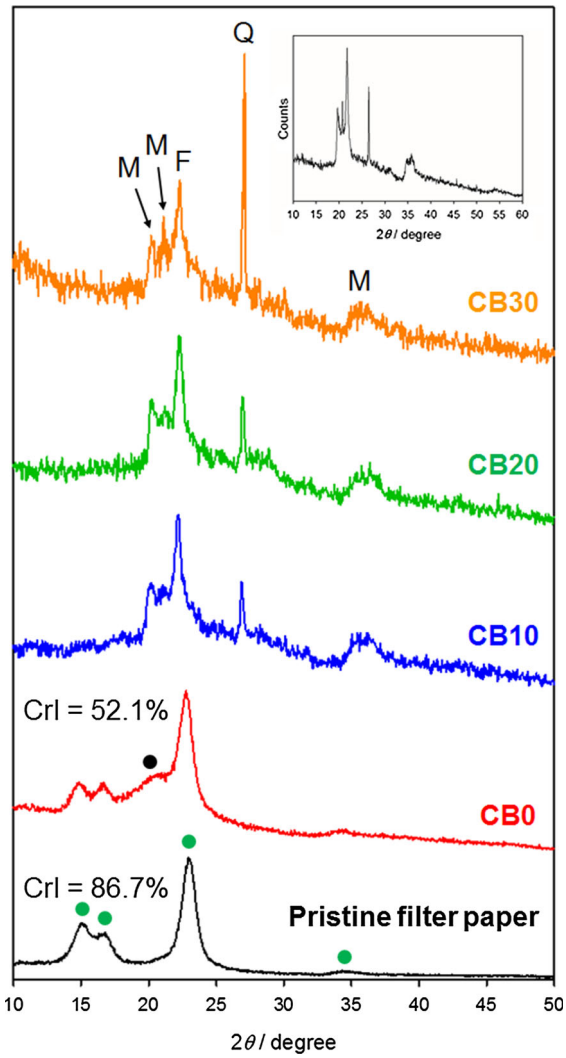

Fig. 5 XRD patterns of pristine cellulose filter paper and CB hydrogels. Inset shows the diffraction pattern of bentonite. CrI denotes the cellulose crystallinity index estimated by the XRD peak height method after baseline subtraction of the spectrum. Symbols "M", "F", and "Q" mark montmorillonite, feldspar, and quartz peaks, respectively. Green and black circles denote the Bragg reflections corresponding to cellulose I and cellulose II, respectively

confirmed by EDX elemental analysis. The corresponding SEM–EDX spectra and elemental maps of pristine filter paper and CB hydrogels are shown in Supplemental Figure S2 and S3, respectively. The characteristic peaks attributed to C and O elements are detected in filter paper and CB0 hydrogel, which is due to the contribution of cellulose component. After the incorporation of bentonite clay, the signals of Si, Mg, and Al elements can be clearly detected in the EDX spectra of CB10, CB20, and CB30 samples, thus confirming the successful formation of the composite hydrogels. The SEM–EDX elemental maps of Si, Al, and Mg also show that these metal species present in bentonite are distributed almost uniformly inside the composite hydrogel matrix.

XRD analysis

The XRD patterns of pristine cellulose filter paper and the prepared hydrogels are displayed in Fig. 5. From this figure, the diffraction peaks observed in the XRD patterns of pristine cellulose filter paper and CB0 hydrogel are related to the cellulose I and II crystal structures. The strong reflection at $2\theta = 22.8°$ and a broad hump-like peak at $2\theta = 14°–18°$ in pristine filter paper can be assigned to the (200), $(1\bar{1}0)$, and (110) crystal planes of cellulose I, respectively (Cai and Zhang 2005; Novo et al. 2015). Another weak Bragg reflection at $2\theta = \sim 34°$ can be attributed to the (040) crystal plane of cellulose I (Novo et al. 2015; Xu et al. 2013). The typical XRD pattern of CB0 hydrogel agrees well with literature reports for cellulose I (Guo et al. 2013; Novo et al. 2015; Xu et al. 2013), showing a strong Bragg peak at $2\theta = 22°–23°$ and an amorphous broad hump at 14°–18°. Moreover, a shoulder appeared at $2\theta = \sim 20°$ can be assigned to the characteristic diffraction peak from cellulose II (plane 110). The coexistence of cellulose I and cellulose II in CB0 hydrogel could be attributed to the partial dissolution of cellulose in alkali/urea aqueous solution. The optical microscope image of the cellulose solution shown in Supplementary Figure S4 revealed that some of the native cellulose fibers were not completely dissolved in a pre-cooled NaOH/urea solution after stirring for 30 min at room temperature. A similar result was obtained by Qi et al. (2011) who investigated the crystal structure of cellulose regenerated from the solution prepared by direct dissolution in 7 wt% NaOH/12 wt% urea aqueous solution at 0 °C. In addition, the extent of the cross-linking reaction directly affects the cellulose crystallinity in the resulting hydrogel. On the basis of the XRD results, the CrI values are found to be 86.7 and 52.1% for pristine cellulose filter paper and CB0 hydrogel, respectively. The decrease in CrI from 86.7 to 52.1% upon the formation of hydrogel could be ascribed to the cross-linking of free cellulose chains with ECH,

which restricts the molecular mobility and the ability of the cellulose molecules to rearrange into an ordered crystalline structure. However, it should be noted here that the initial crystalline structure of cellulose is partially preserved during the cross-linking reaction with ECH, which gives rise to the coexistence of cellulose I and cellulose II.

The diffraction peaks observed in the XRD patterns of CB10, CB20, and CB30 samples arise mainly from the contribution of bentonite particles. In this case, the Bragg peaks at $2\theta = 20.2°$, 21.1°, and 35.8° correspond to the (020), (220), and (200) crystal planes of montmorillonite ($MgO{\cdot}AlO_3{\cdot}5SiO_2{\cdot}H_2O$, JCPDS File No. 00-003-0010) present in bentonite. Meanwhile, the sharp Bragg peaks at $2\theta = 22.3°$ and 27.1° correspond to the (110) and (101) crystal planes of feldspar and quartz (JCPDS File No. 33-1161) phases, respectively (Silva et al. 2018). It can also be seen that the intensity of the (101) quartz diffraction peak increased with increasing clay content from 10 to 30 wt%. On the other hand, the disappearance of the diffraction peaks at $2\theta = 14.3°$ and 22.6° confirmed the disruption of the crystalline structure of cellulose during the dissolution and cross-linking processes in the presence of bentonite particles.

Thermal degradation behavior

Thermal degradation behavior of the prepared hydrogels was investigated by TGA in a nitrogen atmosphere and the results are presented in Table 2. The corresponding TGA curves of all hydrogels are depicted in Supplemental Figure S5. From the figures, it can be seen that all hydrogels exhibited two stages of weight loss in the temperature range 30–600 °C. The initial stage of weight loss occurring in the temperature range of 50–100 °C was attributed to the evaporation of moisture. The moisture content of the pristine filter paper, CB0, CB10, CB20, and CB30 samples was found to be 5.8, 9.6, 8.4, 8.1, and 7.9 wt%, respectively. In this case, the moisture content of the hydrogels was relatively higher than that of pristine filter paper because of the ability of the hydrogel to retain water molecules more strongly.

The second stage of weight loss for CB0 hydrogel occurred at a lower temperature range (190–406 °C) compared to that of pristine filter paper (239–420 °C). This is likely due to the disrupted hydrogen bond network in the hydrogel structure, which is more susceptible to thermal degradation than the intact hydrogen bond network of cellulose in filter paper. The decrease in thermal degradation temperature might also relate to a lower degree of cellulose crystallinity of the sample, as corroborated by XRD analysis. Meanwhile, the second stage of weight loss of 19.8, 15.3, and 10.9% for CB10, CB20, and CB30 samples, respectively took place at higher temperatures than those of pristine filter paper and CB0 hydrogel. The increase in the onset degradation temperature was attributed to the presence of bentonite particles in the hydrogel matrix that can protect heat insulation and subsequently hamper the thermal

Table 2 Thermogravimetric results of cellulose filter paper and CB hydrogels

Sample	Stage	Temperature range (°C)	T_{max}^{a} (°C)	Mass loss (%)	Assignment	Final residue[b]
Filter paper	1	50–97	360.1	5.8	Loss of H_2O	Char (7.8%)
	2	239–420		83.6	Loss of cellulose	
CB0	1	50–113	336.2	9.6	Loss of H_2O	Char (13.6%)
	2	190–406		80.1	Loss of cellulose	
CB10	1	50–98	358.5	8.4	Loss of H_2O	Char (69.4%)
	2	284–427		19.8	Loss of cellulose	
CB20	1	50–109	361.3	8.1	Loss of H_2O	Char (71.8%)
	2	290–427		15.3	Loss of cellulose	
CB30	1	50–109	356.0	7.9	Loss of H_2O	Char (76.5%)
	2	301–421		10.9	Loss of cellulose	

[a]The maximum degradation temperature measured by the derivative TGA curves

[b]The values inside the bracket represent the fraction of the residue remaining at 600 °C

Table 3 Assignment of the IR spectra of surface functional groups present on the pristine filter paper and CB hydrogels

Band assignments		Wavenumber (cm^{-1})				
		Filter paper	CB0	CB10	CB20	CB30
C-H		413	417	413	424	413
Si–O	Bending	–	–	467	463	463
Al–O–Si	Bending	–	–	467	463	463
C–H	Bending	606	565	–	–	–
Fe(II)–Fe(III)–OH	Bending	–	–	791	787	791
C–O/C–C	Stretching	1038	1034	1026	1031	1023
O–H	Bending	1596	1597	1605	1636	1601
C–H ($–CH_2–$)	Stretching	2905	2900	2857	2883	2916
O–H	Stretching	3342	3339	3376	3371	3376

degradation of cellulose. In addition, the thermal decomposition rate of CB10, CB20, and CB30 samples was less compared to the cellulose filter paper and CB0 hydrogel since bentonite particles are thermally stable up to temperatures about 600 °C and are not easily degraded compared to cellulose. CB30 sample has the lowest weight loss at the second stage (10.9%) since this hydrogel sample contains higher bentonite loading than CB10 and CB20 samples.

ATR-FTIR analysis

The surface functional groups of the hydrogels and their corresponding band assignments are summarized in Table 3. The ATR-FTIR spectra of the samples are presented in Supplemental Figure S6. As shown in this figure, the absorption peaks at wavenumbers 413 and 417 cm^{-1} present in the spectra of pristine filter paper and CB0 hydrogel correspond to the bending mode of C-H groups in the cellulose structure. This band, however, decreased in intensity for CB10, CB20, and CB30 samples. The peak attributed to the Al–O–Si bending mode at 542 cm^{-1} represents the octahedral surface of the bentonite layer (Kurniawan et al. 2011; Soetaredjo et al. 2011; Ismadji et al. 2016). Moreover, the presence of bentonite particles was also confirmed by the vibration band of Si–O bending at 467, 463, and 463 cm^{-1} for CB10, CB20, and CB30, respectively. Other vibrational modes in the IR spectra of CB10, CB20, and CB30 hydrogels at wavenumbers greater than 1000 cm^{-1} are similar to that of CB0 hydrogel, indicating no direct interaction between the bentonite particles and dissolved cellulose fibers that lead to the shifts in vibrational band positions and/or alteration of the functional groups. This suggests that the bentonite particles do not participate in the cross-linking reaction with cellulose chains and/or ECH, but rather embedded in-between the cross-linked cellulose networks.

Kinetic, isotherm, and thermodynamic studies of CR adsorption onto CB hydrogels

Kinetic studies

The adsorption of CR dye onto CB hydrogels as a function of time was studied at pH 7 and 30 °C with an initial dye concentration of 50 mg L^{-1}. With respect to the target dye pollutant, the acidic and alkaline pH conditions cause the color of CR solution to turn dark blue and dark red, respectively where the ionized dye molecules in solution carry positive and negative charge (see Supplemental Figure S7 for the digital photographs of CR solutions under different pH conditions as well as the cationic and anionic forms of the dye). The pK_a value of CR in aqueous solution was 5.5 where neutral and alkaline pH conditions cause the dye molecules to exist primarily in anionic form (Purkait et al. 2007). Therefore, the anionic form of the dye molecules was expected to facilitate fast and efficient adsorption onto positively charged hydrogel surface, due to the electrostatic interaction between two oppositely charged surfaces. The Lagergren pseudo-first-order (Lagergren 1898) and pseudo-second-order (Blanchard et al. 1984) models were used to fit experimental kinetic data. The Lagergren pseudo-first-order kinetics is described by Eq 4:

$$q_t = q_e\left[1 - \left(e^{-k_1 t}\right)\right] \quad (4)$$

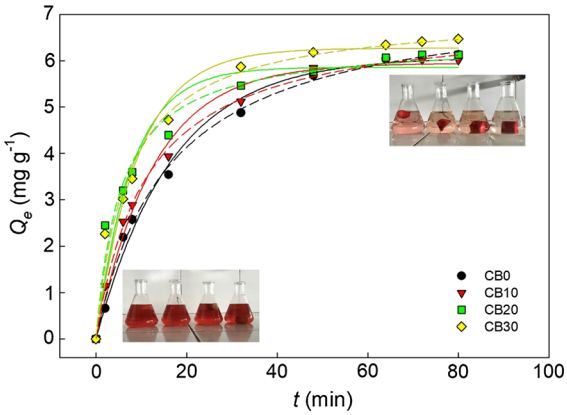

Fig. 6 Adsorption kinetics of CR onto CB hydrogels at pH 7 and 30 °C. The colored solid and dashed lines represent fits to the pseudo-first-order and pseudo-second-order equations, respectively; symbols represent experimental data. The inset images show the photographs of the dye solutions with bulk hydrogels before (bottom) and after (top) adsorption

The pseudo-second-order kinetic model is given by Eq 5:

$$q_t = q_e\left(\frac{q_e k_2 t}{1 + q_e k_2 t}\right) \tag{5}$$

where q_t and q_e are the amount adsorbed at time t and at equilibrium (mg g^{-1}), respectively. The fitting parameters k_1 and k_2 in Eqs. 4 and 5 represent the pseudo-first-order (min^{-1}) and the pseudo-second-order rate coefficients (g mg^{-1} min^{-1}), respectively.

The fitting of pseudo-first-order and pseudo-second-order kinetic models to experimental data is displayed in Fig. 6 and the fitting parameters (k and q_e) of both models are shown in Table 4. With respect to the correlation coefficient (R^2) values, the experimental kinetic data were found to fit better to the pseudo-second-order model. Based on this kinetic model, it was found that the rate of CR adsorbed onto hydrogels (k_2) as well as the equilibrium dye adsorption capacity (q_e) are marginally increased with increasing bentonite content. Higher values of k_2 and q_e denote that the incorporation of bentonite particles provides structure and higher number of available adsorption sites on the surface of hydrogels for anionic dye molecules. Among the prepared CB hydrogels, CB30 sample exhibited the best adsorption capacity toward CR dye, followed by CB20, CB10, and CB0 samples.

Equilibrium isotherm studies

The adsorption equilibrium data of CR onto CB hydrogels at various temperatures are displayed in Fig. 7. Even though Langmuir model was theoretically adequate to represent adsorption equilibrium data (based on the BET analysis), it is still interesting to observe how the data fit to the Freundlich model. Langmuir is a classic adsorption model that assumes a monolayer and homogeneous adsorption at specific sites on the adsorbent surface (Langmuir 1916). The Langmuir equation is described by Eq 6:

$$q_e = q_{max}\frac{K_L C_e}{1 + K_L C_e} \tag{6}$$

The Freundlich model is widely used to represent the adsorption equilibria of organic and inorganic compounds onto various types of adsorbents (Freundlich 1932). This model, however, has no restriction on monolayer adsorption and a limit in adsorption capacity as in the Langmuir model. The mathematical expression of Freundlich adsorption isotherm is given by Eq 7:

$$q_e = K_F C_e^{1/n} \tag{7}$$

where q_e is the amount of solute adsorbed per gram of adsorbent at equilibrium (mg g^{-1}), C_e is the solute concentration in solution at equilibrium (mg L^{-1}); in

Table 4 The values of the fitting parameters obtained for pseudo-first-order and pseudo-second-order models for the CR adsorption onto CB hydrogels

Adsorbent	Pseudo-first-order			Pseudo-second-order		
	k_1 (min^{-1})	q_e (mg g^{-1})	R^2	k_2 (g mg^{-1} min^{-1})	q_e (mg g^{-1})	R^2
CB0	0.06	5.58	0.99	0.01	6.48	0.99
CB10	0.08	5.86	0.99	0.01	6.76	0.99
CB20	0.13	5.98	0.94	0.03	6.78	0.98
CB30	0.11	6.27	0.97	0.02	7.03	0.98

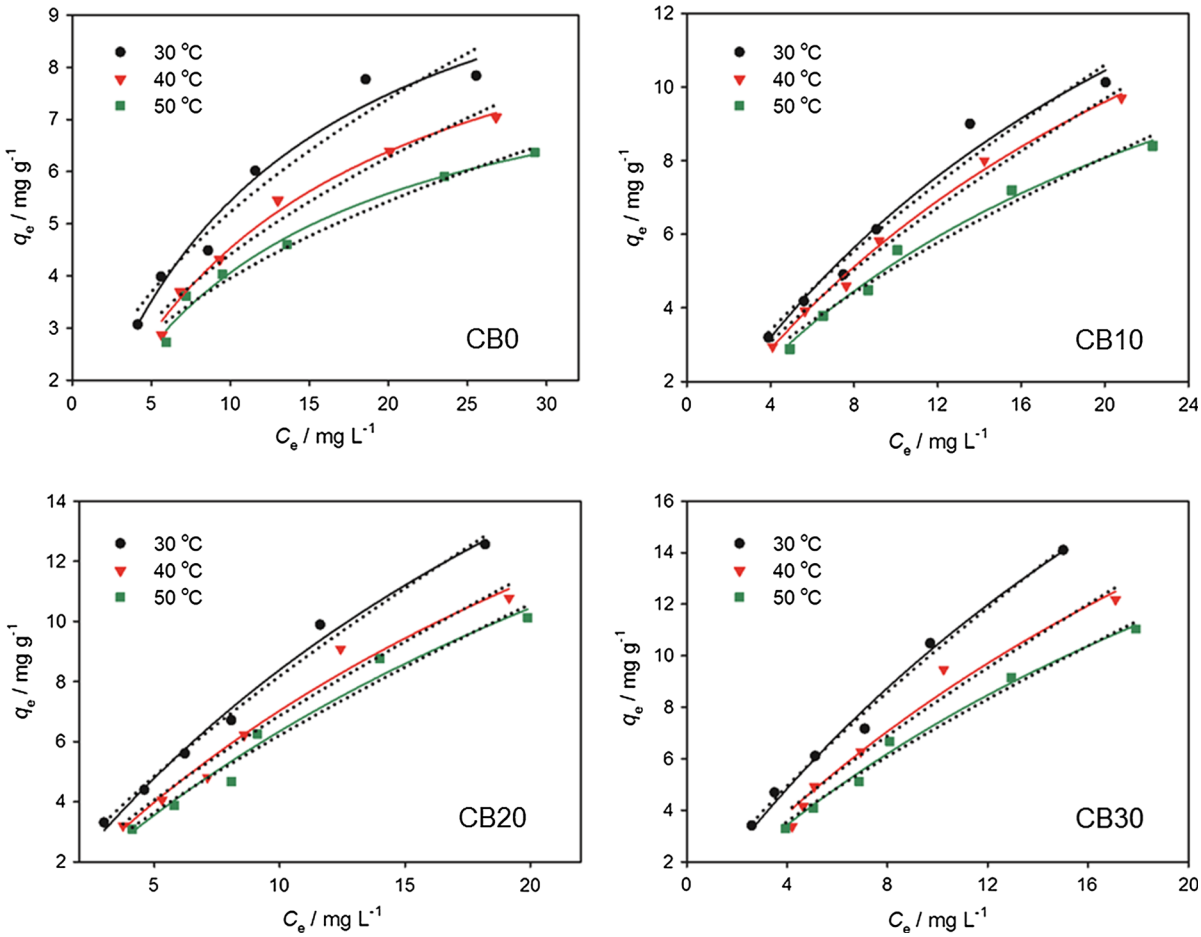

Fig. 7 The equilibrium adsorption isotherms of CR onto CB hydrogels at 30, 40, and 50 °C. The solid-colored and black dotted lines represent fits to the Langmuir and Freundlich isotherm models, respectively; symbols represent experimental data

the Langmuir model, the constant q_{max} corresponds to the theoretical maximum (monolayer) adsorption capacity of the solute on the solid (mg g^{-1}) and K_L represents the Langmuir constant related to the adsorption affinity (L mg^{-1}). In the Freundlich model, the constant K_F denotes the Freundlich parameter corresponding to the adsorption capacity $(\text{mg g}^{-1})(\text{mg L}^{-1})^{-n}$ and $1/n$ (dimensionless) is the heterogeneity factor characterizing adsorption intensity and surface heterogeneity. In this case, the value of n should fall between 1 and 10 for favorable adsorption conditions (Ai et al. 2011). Additionally, the essential characteristic of the Langmuir isotherm can be expressed in terms of a dimensionless constant called separation factor or equilibrium parameter R_L, which is defined by Eq 8:

$$R_L = \frac{1}{1 + K_L C_0} \tag{8}$$

where C_0 represents the initial adsorbate concentration (mg L^{-1}). The values of R_L indicate the shape of the adsorption isotherm to be either unfavorable ($R_L > 1$), linear ($R_L = 1$), favorable ($0 < R_L < 1$), or irreversible ($R_L = 0$) (Weber and Chakravorti 1974).

The fitting of adsorption equilibrium data to the Langmuir and Freundlich isotherm models is depicted in Fig. 7. The results indicated that the extent of dye removal decreased with increasing temperature from 30 to 50 °C, which suggests that the sorption process follows a typical physisorption behavior and is exothermic in nature. Similar observations were also found for the adsorption of CR onto cattail root (Hu et al. 2010), chitosan hydrobeads (Chatterjee et al.

2007), and clay materials (Vimonses et al. 2009), as well as for the adsorption of acid red 88 dye onto multiwalled carbon nanotubes-Fe_3C nanocomposite (Konicki et al. 2014). The phenomenon of declining adsorption with an increase in temperature indicates the weakening of physical attractive forces between dye molecules and the surface sites of the adsorbent. The decline in the adsorption capacity with increasing temperature can also be explained by the solubility effect of the adsorbate (Bartell et al. 1951). In this case, the chemical potential of the adsorbate becomes lower at higher temperature as a consequence of an increased solubility of the dye, which in turn retards the adsorption process. Moreover, increasing temperature may also decrease the swelling degree of the hydrogel as previously reported by Westman and Lindström (1981), which could impede the adsorption due to less space for the diffusion and loading of the dye molecules into the interior of the CB hydrogels; at lower equilibrium temperature the swelling degree is higher, and thus, the dye molecules can diffuse more rapidly and their physical interactions with the surface can be more strongly held. The larger degree of swelling could enhance the adsorption capacity, as demonstrated by Chen et al. (2016). The fitting parameters of Langmuir and Freundlich models obtained from a nonlinear least-squares analysis are summarized in Table 5. As can be seen, the Langmuir adsorption isotherm represents the experimental data better than the Freundlich isotherm as indicated by the higher R^2 values, thus confirming the BET analysis and the monolayer adsorption of CR on the hydrogel surface.

The Langmuir model parameter, q_{max}, indicates that the highest monolayer adsorption capacity was obtained for CB30 hydrogel. The theoretical maximum adsorption capacity of the CB hydrogels can be ranked as follows: CB30 > CB20 > CB10 > CB0 where the q_{max} values at 30 °C are 45.77, 34.03, 24.20, and 12.00 mg g^{-1}, respectively. Compared with pure cellulose hydrogel, CB10, CB20, and CB30 samples exhibited a 2- to almost fourfold increase in the q_{max} values. Meanwhile, the q_{max} value of bentonite was found to be 20.97 mg g^{-1}, which was lower than those obtained for the composite hydrogels. These results suggest that the incorporation of bentonite particles into the hydrogel matrix resulted in a remarkable improvement in the dye adsorption capacity. It is expected that the incorporation of bentonite particles into the cellulose network provides established higher surface area and sites, thus promoting the CR adsorption. Also, as can be seen from Table 6, the adsorption capacity of CB30 hydrogel (45.77 mg g^{-1}) is comparable to those of other reported adsorbents used for removal of CR, such as chitosan/cellulose hydrogel (47.32 mg g^{-1}) (Tu et al. 2017), cellulose/chitosan hydrogel beads (40.0 mg g^{-1}) (Li et al. 2015), and DAMFC/chitosan composite film (56.90 mg g^{-1}) (Zheng et al. 2018), but higher than those derived from agricultural residues (Annadurai et al. 2002; Wang and Chen 2009; Kumar et al. 2010; Dawood and Sen 2012; Roy et al. 2013). Although the

Table 5 Langmuir and Freundlich isotherm parameters for the CR adsorption onto CB hydrogels

Adsorbent	q_{max} (mg g^{-1})			K_L (× 10^{-2} L mg^{-1})			R^2		
	30 °C	40 °C	50 °C	30 °C	40 °C	50 °C	30 °C	40 °C	50 °C
CB0	12.00	10.80	8.91	8.29	7.24	6.38	0.97	0.99	0.98
CB10	24.20	21.06	17.62	3.80	3.56	3.23	0.98	0.99	0.99
CB20	34.03	29.97	23.49	3.27	3.02	2.74	0.97	0.98	0.97
CB30	45.77	38.82	31.97	2.95	2.71	2.44	0.99	0.98	0.99
Adsorbent	K_F (mg g^{-1}) (mg L^{-1})$^{-n}$			n			R^2		
	30 °C	40 °C	50 °C	30 °C	40 °C	50 °C	30 °C	40 °C	50 °C
CB0	1.65	1.37	1.38	2.00	1.97	2.19	0.95	0.96	0.98
CB10	1.27	1.14	1.12	1.41	1.40	1.51	0.96	0.98	0.98
CB20	1.44	1.20	1.06	1.33	1.32	1.30	0.98	0.97	0.97
CB30	1.63	1.30	1.22	1.25	1.25	1.30	0.99	0.96	0.98

Table 6 Comparison of the adsorption capacity of several agricultural byproducts and polysaccharide-based composite adsorbents for removal of CR dye

Adsorbent	Characteristic	pH	T (K)	q_{max} (mg g^{-1})	References
DAMFC/chitosan composite film	NS	5.5	NS	56.90	Zheng et al. (2018)
HAp-chitosan composite	Chemisorption	NS	room	769.0	Hou et al. (2012)
Chitosan hydrobeads	Physisorption	6.0	303	93.71	Chatterjee et al. (2007)
Chitosan/cellulose hydrogel	NS	NS	room	47.32	Tu et al. (2017)
Cellulose/chitosan hydrogel beads	NS	NS	298	40.0	Li et al. (2015)
PEI-modified wheat straw	Chemisorption	5.0	303	89.70	Shang et al. (2016)
PEG-PAA-bentonite composite hydrogel	Physisorption	7.0	298	110.0	Bhattacharyya and Ray (2015)
Cashew nut shell	Chemisorption	3.0	303	5.18	Kumar et al. (2010)
Pine cone	Chemisorption	3.6	303	32.65	Dawood and Sen (2012)
Tannin-grafted jute fiber	Physisorption	3.0	303	27.12	Roy et al. (2013)
CCDA	Physisorption	4.0	310	34.70	Kumari et al. (2016)
Rice bran	Chemisorption	8.0	298	14.63	Wang and Chen (2009)
Orange peel	NS	> 7.0	303	14.0	Annadurai et al. (2002)
CB30 hydrogel	Physisorption	7.0	303	45.77	This work

DAMFC dialdehyde microfibrillated cellulose, *Hap* hydroxyapatite, *PEI* polyethyleneimine, *PEG-PAA* solution polymerization of polyethylene glycol and poly(acrylic acid), *CCDA* crosslinked cellulose dialdehyde, *NS* not specified

adsorption capacity of CB30 hydrogel is much lower than those of HAp-chitosan composite (769 mg g^{-1}) (Hou et al. 2012) and PEG-PAA-bentonite composite hydrogel (110 mg g^{-1}) (Bhattacharyya and Ray 2015), their preparation, however, are either complex or time-consuming and involve multiple procedures. On the other hand, the present CB30 hydrogel is relatively easy and cheap to prepare in large quantities from sustainable raw materials, thus showing great potential for practical application in dye removal especially when process costs are taken into account. Moreover, the CR adsorption onto CB30 hydrogel occurs favorably without further pH adjustment, which makes the process scale-up simpler and less costly. The low adsorption affinity constant, K_L, indicates there is no strong interaction between the adsorbate and the adsorbent, thus confirming the physisorption process of CR adsorption onto CB hydrogels. In addition, the values of R_L ranged between 0.2 and 0.5 for all of the systems studied (see Supplemental Figure S8), confirming the favorability of the adsorption process.

Thermodynamic studies

Adsorption thermodynamics can provide in-depth information regarding the type and mechanism of an adsorption process, which is particularly useful for the industrial process design and scale-up. The thermodynamic parameters for the adsorption process, such as the changes in the Gibbs free energy ($\Delta G°$, kJ mol^{-1}), enthalpy ($\Delta H°$, kJ mol^{-1}), and entropy ($\Delta S°$, J mol^{-1} K^{-1}) were determined using the van't Hoff equation describing the relationship between the thermodynamic equilibrium constant of adsorption (K_a) and temperature as follows:

$$\ln K_a = -\frac{\Delta H^{\circ}}{RT} + \frac{\Delta S^{\circ}}{R} \quad (9)$$

In Eq 9, K_a can be obtained by plotting ln (q_e/C_e) versus q_e and extrapolating q_e to zero (Ma et al. 2012), T is the absolute temperature (K), and R is the universal gas constant (8.314 J mol^{-1} K^{-1}). According to Liu (2009), the use of the Langmuir equilibrium constant (K_L) for calculation of $\Delta G°$, $\Delta H°$, and $\Delta S°$ of adsorption is acceptable since K_a can be reasonably approximated by K_L for the case of either a dilute solution of charged adsorbate or a solution of uncharged adsorbate at any concentration. The values of $\Delta H°$ and $\Delta S°$ can be calculated from the slope and intercept of a linear plot of ln K_a versus $1/T$, respectively (see Supplemental Figure S9). The Gibbs free energy of adsorption was calculated from K_a using Eq 10:

Table 7 Thermodynamic parameters for the adsorption of CR onto CB hydrogels at different temperatures

Adsorbent	$\Delta G°$ (kJ mol^{-1})			$\Delta H°$ (kJ mol^{-1})	$\Delta S°$ (J mol^{-1} K^{-1})
	30 °C	40 °C	50 °C		
CB0	− 28.55	− 29.14	− 29.73	− 10.67	58.97
CB10	− 26.58	− 27.29	− 27.90	− 6.60	65.94
CB20	− 26.20	− 26.86	− 27.46	− 7.19	62.73
CB30	− 25.94	− 26.58	− 27.15	− 7.72	60.14

$$\Delta G^{\circ} = -RT \ln K_{a} \quad (10)$$

The obtained thermodynamic parameters for the CR adsorption onto CB hydrogels are summarized in Table 7. From this table, it can be seen that the $\Delta G°$ values are negative at all temperatures, characterizing the spontaneous nature and the feasibility of the adsorption process. Moreover, the more negative values of $\Delta G°$ indicate that the adsorption process becomes thermodynamically more favorable with increasing temperature. Meanwhile, the negative value of $\Delta H°$ suggests an exothermic adsorption process and the dye adsorption onto hydrogels was governed by physical adsorption since all the $\Delta H°$ values fall within the range of 2.1 to 20.9 kJ mol^{-1} (Liu 2009). Physical adsorption of CR onto CB hydrogels may involve weak attractive forces, such as hydrogen bonding and van der Waals force. The positive $\Delta S°$ values of CB hydrogels suggest an increased randomness at the solid-solution interface during the adsorption of dye molecules onto hydrogel (Vimonses et al. 2009).

Seed germination and seedling growth in *Vigna radiata* L. and *Arabidopsis thaliana*

The porous and self-standing features of CB hydrogels could show potential as substrates for soilless culture. In this regard, the ability of CB hydrogels to promote germination and growth of seedlings was evaluated in the model plant mung bean (*Vigna radiata* L.) and mouse-ear cress (*Arabidopsis thaliana*). In a typical procedure shown in Fig. 8, the prepared hydrogels were soaked in tap water until used in germination tests. Subsequently, the plant seeds were spread uniformly on the surface of the hydrogels and then germinated under sunlight exposure for up to 5 days. After 5 days, it was found that the seedlings of *Vigna radiata* L. grow well on the hydrogel surface and had fully expanded leaves and cotyledons on the main stem, as shown in Fig. 8c. Moreover, the plant roots can easily penetrate deeply into the hydrogel matrix (Fig. 8b), indicating soft porous environment of CB hydrogels. It is also observed that the extent of root growth in CB10 and CB20 hydrogels was greater compared with that of CB0 hydrogel. This implies that

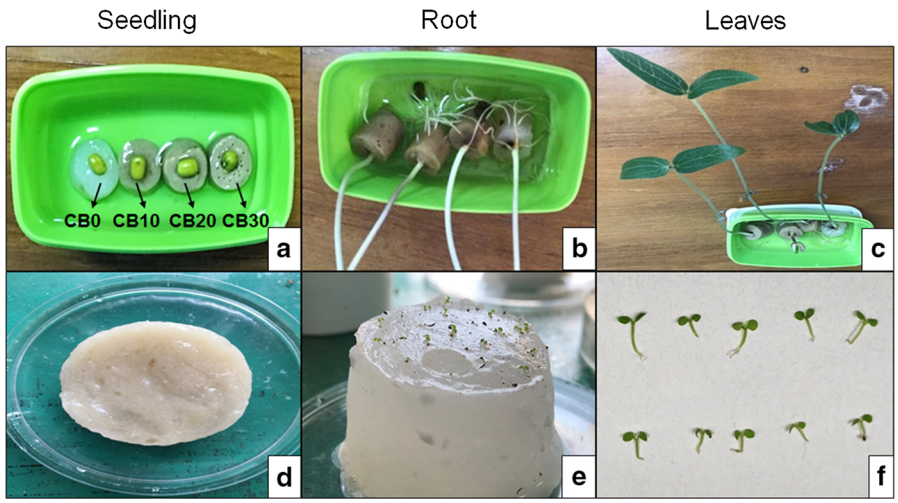

Fig. 8 Seed germination assays for *Vigna radiata* L. (panels **a**–**c**) and *Arabidopsis thaliana* (panels **d**–**f**) on the surface of CB hydrogels: Panels b and e are typical leaf growth in *Vigna radiata* L. and Arabidopsis after 5 days, respectively. Panels c and f show root development of 5-day-old seedlings of *Vigna radiata* L. and Arabidopsis, respectively. For Arabidopsis (bottom panels), the seedlings were grown on CB20 hydrogel

bentonite particles embedded in the hydrogel matrix can provide a hydrated microenvironment to promote seed shell swelling and germination. In addition, the presence of the divalent Fe^{2+} and Mg^{2+} cations in the octahedral sheet of the clay layer can serve as a source of plant nutrients for enhancing rooting activity of the seedling. However, further increasing the loading of bentonite to 30 wt% leads to a decrease in primary root growth and lateral root formation compared to 10 and 20 wt% clay loadings. This result could be attributed to the increased structural rigidity of the composite hydrogel with bentonite additions, which provide mechanical resistance to root growth. On the other hand, the growth of Arabidopsis seedlings on CB20 hydrogel (Fig. 8d) was considerably slower than that of *Vigna radiata* L. and after 5 days, most of the seedlings are still in sprouts, as shown in Fig. 8e. As can be seen, the Arabidopsis primary roots did not grow to the same extent as in the *Vigna radiata* L. and they are not strong enough to penetrate inside the hydrogel matrix (Fig. 8f), thus hampering the growth of whole plant. However, green cotyledons and stem can still be observed on 5-day-old grown seedlings. These results demonstrated the feasibility of CB hydrogels for seed germination before transferring to soil media. For legume plants, such as *Vigna radiata* L., the fabricated composite hydrogels can also be used as a growth medium instead of soil or agar.

Conclusions

In this work, porous composite hydrogels prepared from cellulose filter paper and bentonite clay have been successfully employed as a low cost and eco-friendly adsorbent for effective removal of CR from aqueous solution. The formation of CB hydrogels was confirmed by the alteration on and properties such as surface, crystallinity, thermal degradation behavior, and functional groups compared to the raw cellulose fiber from filter paper. The potential of the CB hydrogels has been tested to remove CR at neutral pH and different temperatures. The results demonstrated that the studied dye molecules adsorbed on CB hydrogels by physisorption, where CB30 hydrogel exhibited the highest monolayer adsorption capacity (45.77 mg g^{-1}) compared to those of cellulose composite hydrogels with lower bentonite mass loading. It was found that both the normal temperature and the solubility effects synergistically contribute to the decrease in dye adsorption capacity at elevated temperature. Thermodynamic studies revealed that the adsorption of CR onto CB hydrogels was a spontaneous exothermic process. To this end, the prepared CB hydrogels can be potentially applied in agriculture as nonsoil media to promote seed germination and normal growth of *Vigna radiata* L. and to a lesser extent *Arabidopsis thaliana*.

Acknowledgments The authors gratefully acknowledge the funding from Widya Mandala Surabaya Catholic University with a Contract Number 3940/WM01/N/2017. The authors also thank National Taiwan University of Science and Technology (Taiwan Tech) for providing facility for material characterization.

References

Adzmi F, Meon S, Musa MH, Yusuf NA (2012) Preparation, characterization and viability of encapsulated *Trichoderma harzianum* UPM40 in alginate-monmorillonite clay. J Microencapsul 29:205–210

Ahmed EM (2015) Hydrogel: preparation, characterization, and applications: a review. J Adv Res 6:105–121

Ai L, Zhang C, Meng L (2011) Adsorption of methyl orange from aqueous solution on hydrothermal synthesized Mg–Al layered double hydroxide. J Chem Eng Data 56:4217–4225

Annadurai G, Juang RS, Lee DJ (2002) Use of cellulose-based wastes for adsorption of dyes from aqueous solutions. J Hazard Mater B92:263–274

Bahranowski K, Gawel A, Klimek A, Michalik-Zym A, Napruszewska BD, Nattich-Rak M, Rogowska M, Serwicka EM (2017) Influence of purification method of Na-montmorillonite on textural properties of clay mineral composites with TiO_2 nanoparticles. Appl Clay Sci 140:75–80

Bartell FE, Thomas TL, Fu Y (1951) Thermodynamics of adsorption from solutions. IV. Temperature dependence of adsorption. J Phys Chem 55:1456–1462

Bhattacharya S, Das A, Mangai G, Vignesh K, Sangeetha J (2011) Mycoremediation of congo red dye by filamentous fungi. Braz J Microbiol 42:1526–1536

Bhattacharyya R, Ray SK (2015) Removal of congo red and methyl violet from water using nano clay filled composite hydrogels of poly acrylic acid and polyethylene glycol. Chem Eng J 260:269–283

Blanchard G, Maunaye M, Martin G (1984) Removal of heavy metals from waters by means of natural zeolites. Water Res 18:1501–1507

Blasko A, Bunton CA, Bunel S, Ibarra C, Moraga E (1997) Determination of acid dissociation constants of anomers of amino sugars by ^{1}H NMR spectroscopy. Carbohydr Res 298:163–172

Brunauer S, Emmett PH, Teller E (1938) Adsorption of gases in multimolecular layers. J Am Chem Soc 60:309–319

Cai J, Zhang L (2005) Rapid dissolution of cellulose in LiOH/urea and NaOH/urea aqueous solutions. Macromol Biosci 5:539–548

Chang C, Zhang L (2011) Cellulose-based hydrogels: present status and application prospects. Carbohydr Polym 84:40–53

Chatterjee S, Chatterjee S, Chatterjee BP, Guha AK (2007) Adsorptive removal of congo red, a carcinogenic textile dye by chitosan hydrobeads: binding mechanism, equilibrium and kinetics. Colloids Surf A 299:146–152

Chen D, Wang L, Ma Y, Yang W (2016) Super-adsorbent material based on functional polymer particles with a multilevel porous structure. NPG Asia Mater 8:e301

Daraei P, Madaeni SS, Salehi E, Ghaemi N, Ghari HS, Khadivi MA, Rostami E (2013) Novel thin film composite membrane fabricated by mixed matrix nanoclay/chitosan on PVDF microfiltration support: preparation, characterization and performance in dye removal. J Membr Sci 436:97–108

Dawood S, Sen TK (2012) Removal of an anionic dye Congo red from aqueous solution by raw pine and acid-treated pine cone powder as adsorbent: equilibrium, thermodynamic, kinetics, mechanism and process design. Water Res 46:1933–1946

Demitri C, Giuri A, Raucci MG, Giugliano D, Madaghiele M, Sannino A, Ambrosio L (2014) Preparation and characterization of cellulose-based foams via microwave curing. Interface Focus 4:20130053

Freundlich H (1932) Of the adsorption of gases. Section II. Kinetics and energetics of gas adsorption. Introductory paper to section II. Trans Faraday Soc 28:195–201

Guo B, Chen W, Yan L (2013) Preparation of flexible, highly transparent, cross-linked cellulose thin film with high mechanical strength and low coefficient of thermal expansion. ACS Sustain Chem Eng 1:1474–1479

Holmberg L, Lindberg B, Lindqvist B (1994) The reaction between epichlorohydrin and polysaccharides: Part 1, syntheses of some model substances with non-cyclic substituents. Carbohydr Res 262:213–221

Hou H, Zhou R, Wu P, Wu L (2012) Removal of Congo red dye from aqueous solution with hydroxyapatite/chitosan composite. Chem Eng J 211–212:336–342

Hu Z, Chen H, Ji F, Yuan S (2010) Removal of Congo red from aqueous solution by cattail root. J Hazard Mater 173:292–297

Ismadji S, Tong DS, Soetaredjo FE, Ayucitra A, Yu WH, Zhou CH (2016) Bentonite hydrochar composite for removal of ammonium from Koi fish tank. Appl Clay Sci 119:146–154

Kaşgöz H, Durmus A (2008) Dye removal by a novel hydrogel-clay nanocomposite with enhanced swelling properties. Polym Adv Technol 19:838–845

Konicki W, Pelech I, Mijowska E, Jasinska I (2014) Adsorption kinetics of acid dye Acid Red 88 onto magnetic multi-walled carbon nanotubes-Fe_3C nanocomposite. Clean 42:284–294

Kumar PS, Ramalingam S, Senthamarai C, Niranjanaa M, Vijayalakshmi P, Sivanesan S (2010) Adsorption of dye from aqueous solution by cashew nut shell: studies on equilibrium isotherm, kinetics and thermodynamics of interaction. Desalination 261:52–60

Kumari S, Mankotia D, Chauhan GS (2016) Crosslinked cellulose dialdehyde for Congo red removal from its aquoeus solutions. J Environ Chem Eng 4:1126–1136

Kurniawan A, Sutiono H, Ju YH, Soetaredjo FE, Ayucitra A, Yudha A, Ismadji S (2011) Utilization of rarasaponin natural surfactant for organo-bentonite preparation: application for methylene blue removal from aqueous effluent. Microporous Mesoporous Mater 142:184–193

Lagergren S (1898) About the theory of so-called adsorption of soluble substances. K Sven Vetenskapsakad Handl 24:1–39

Langmuir I (1916) The constitution and fundamental properties of solids and liquids. Part I. Solids. J Am Chem Soc 38:2221–2295

Li M, Wang Z, Li B (2015) Adsorption behaviour of congo red by cellulose/chitosan hydrogel beads regenerated from ionic liquid. Desalin Water Treat 57:16970–16980

Liu Y (2009) Is the free energy change of adsorption correctly calculated? J Chem Eng Data 54:1981–1985

Ma J, Yu F, Zhou L, Jin L, Yang M, Luan J, Tang Y, Fan H, Yuan Z, Chen J (2012) Enhanced adsorptive removal of methyl orange and methylene blue from aqueous solution by alkali-activated multiwalled carbon nanotubes. ACS Appl Mater Interfaces 4:5749–5760

Maitra J, Shukla VK (2014) Cross-linking in hydrogels—a review. Am J Polym Sci 4:25–31

Medjitov DR, Shode LG, Tseitlin GM (1998) Composition of condensation products of bisphenol-A and epichlorohydrin. Polym Bull 40:509–516

Mohammadi-Khoo S, Moghadam PN, Fareghi AR, Movagharnezhad N (2016) Synthesis of a cellulose-based hydrogel network: characterization and study of urea fertilizer slow release. J Appl Polym Sci. https://doi.org/10.1002/app.42935

Montesano FF, Parente A, Santamaria P, Sannino A, Serio F (2015) Biodegradable superabsorbent hydrogel increases water retention properties of growing media and plant growth. Agric Agric Sci Procedia 4:451–458

Novo LP, Bras J, Garcia A, Belgacem N, Curvelo AAS (2015) Subcritical water: a method for green production of cellulose nanocrystals. ACS Sustainable Chem Eng 3:2839–2846

Olsson C, Westman G (2013) Direct dissolution of cellulose: background, means and applications. In: van de Ven T, Godbout L (eds) Cellulose—fundamental aspects. InteChOpen, London, pp 143–178

Pan S, Ragauskas AJ (2012) Preparation of superabsorbent cellulosic hydrogels. Carbohydr Polym 87:1410–1418

Patel H, Vashi RT (2012) Removal of Congo Red dye from its aqueous solution using natural coagulants. J Saudi Chem Soc 16:131–136

Peng N, Hu D, Zeng J, Li Y, Liang L, Chang C (2016) Superasorbent cellulose-clay nanocomposite hydrogels for highly efficient removal of dye in water. ACS Sustain Chem Eng 4:7217–7224

Pham TD, Kobayashi M, Adachi Y (2015) Adsorption of anionic surfactant sodium dodecyl sulfate onto alpha alumina with small surface area. Colloid Polym Sci 293:217–227

Purkait MK, Maiti A, DasGupta S, De S (2007) Removal of congo red using activated carbon and its regeneration. J Hazard Mater 145:287–295

Qi H, Yang Q, Zhang L, Liebert T, Heinze T (2011) The dissolution of cellulose in NaOH-based aqueous system by two-step process. Cellulose 18:237–245

Roy A, Adhikari B, Majumder SB (2013) Equilibrium, kinetic, and thermodynamic studies of azo dye adsorption from aqueous solution by chemically modified lignocellulosic jute fiber. Ind Eng Chem Res 52:6502–6512

Sarkar N, Sahoo G, Das R, Swain SK (2018) Three-dimensional rice straw-structured magnetic nanoclay-decorated tripolymeric nanohydrogels as superadsorbent of dye pollutants. ACS Appl Nano Mater 1:1188–1203

Segal L, Creely JJ, Martin AE, Conrad CM (1959) An empirical method for estimating the degree of crystallinity of native cellulose using the X-ray diffractometer. Text Res J 29:786–794

Shang Y, Zhang J, Wang X, Zhang R, Xiao W, Zhang S, Han R (2016) Use of polyethyleneimine-modified wheat straw for adsorption of Congo red from solution in batch mode. Desalin Water Treat 57:8872–8883

Shen X, Shamshina JL, Berton P, Gurau G, Rogers RD (2016) Hydrogels based on cellulose and chitin: fabrication, properties, and applications. Green Chem 18:53–75

Silva CM, Rosseel TM, Kirkegaard MC (2018) Radiation-induced changes in quartz, a mineral analog of nuclear power plant concrete aggregates. Inorg Chem 57:3329–3338

Sing KSW (1998) Adsorption methods for the characterization of porous materials. Adv Colloid Interface Sci 76–77:3–11

Soetaredjo FE, Ayucitra A, Ismadji S, Maukar AL (2011) KOH/bentonite catalysts for transesterification of palm oil to biodiesel. Appl Clay Sci 53:341–346

Sun XH, Chang XL, Tuo WQ, Wang D, Li KF (2014) Performance comparison of dye-sensitized solar cell by using different metal oxide-coated TiO_2 as the photoanode. AIP Adv 4:1–7

Suwandi AC, Indraswati N, Ismadji S (2012) Adsorption of N-methylated diaminotriphenilmethane dye (malachite green) on natural rarasaponin modified kaolin. Desalin Water Treat 41:342–355

Takács E, Wojnárovits L, Borsa J, Rácz I (2010) Hydrophilic/hydrophobic character of grafted cellulose. Radiat Phys Chem 79:467–470

Tu H, Yu Y, Chen J, Shi X, Zhou J, Deng H, Du Y (2017) Highly cost-effective and high-strength hydrogels as dye adsorbents from natural polymers: chitosan and cellulose. Polym Chem 8:2913–2921

Vimonses V, Lei S, Jin B, Chow CWK, Saint C (2009) Kinetic study and equilibrium isotherm analysis of Congo Red adsorption by clay materials. Chem Eng J 148:354–364

Volzone C, Garrido LB (2001) Changes in suspension properties of structural modified montmorillonites. Ceramica 47:4–8

Wang XS, Chen JP (2009) Biosorption of Congo red from aqueous solution using wheat bran and rice bran: batch studies. Sep Sci Technol 44:1452–1466

Weber TW, Chakravorti RK (1974) Pore and solid diffusion models for fixed-bed adsorbers. AIChE J 20:228–238

Westman L, Lindström T (1981) Swelling and mechanical properties of cellulose hydrogels. III. Temperature effects on the swelling and compliance levels studied by dilatometry and ^{1}H-NMR spectroscopy. J Appl Polym Sci 26:2545–2559

Xu X, Liu F, Jiang L, Zhu JY, Haagenson D, Wiesenborn DP (2013) Cellulose nanocrystals vs. cellulose nanofibrils: a comparative study on their microstructures and effects as polymer reinforcing agents. ACS Appl Mater Interfaces 5:2999–3009

Zhang S, Wang WC, Li FX, Yu JY (2013) Swelling and dissolution of cellulose in NaOH aqueous solvent systems. Cellul Chem Technol 47:671–679

Zheng X, Li X, Li J, Wang L, Jin W, Liu J, Pei Y, Tang K (2018) Efficient removal of anionic dye (Congo red) by dialdehyde microfibrillated cellulose/chitosan composite film with significantly improved stability in dye solution. Int J Biol Macromol 107:283–289